



Article

Transport Characteristics of Fujifilm Ion-Exchange Membranes as Compared to Homogeneous Membranes AMX and CMX and to Heterogeneous Membranes MK-40 and MA-41

Veronika Sarapulova ¹, Inna Shkorkina ¹, Semyon Mareev ¹, Natalia Pismenskaya ^{1,*},
Natalia Kononenko ¹, Christian Larchet ² , Lasaad Dammak ² and Victor Nikonenko ¹ 

¹ Department of Physical Chemistry, Kuban State University, 149 Stavropolskaya st., 350040 Krasnodar, Russia

² Institut de Chimie et des Matériaux Paris-Est, UMR7182 CNRS—Université Paris-Est, 2 rue Henri Dunant, 94320 Thiais, France

* Correspondence: n_pismen@mail.ru; Tel.: +7-918-48-91-292

Received: 15 June 2019; Accepted: 10 July 2019; Published: 14 July 2019



Abstract: Ion-exchange membranes (IEMs) find more and more applications; the success of an application depends on the properties of the membranes selected for its realization. For the first time, the results of a comprehensive characterization of the transport properties of IEMs from three manufactures (Astom, Japan; Shchekinoazot, Russia; and Fujifilm, The Netherlands) are reported. Our own and literature data are presented and analyzed using the microheterogeneous model. Homogeneous Neosepta AMX and CMX (Astom), heterogeneous MA-41 and MK-40 (Shchekinoazot), and AEM Type-I, AEM Type-II, AEM Type-X, as well as CEM Type-I, CEM Type-II, and CEM Type-X produced by the electrospinning method (Fujifilm) were studied. The concentration dependencies of the conductivity, diffusion permeability, as well as the real and apparent ion transport numbers in these membranes were measured. The counterion transport number characterizing the membrane permselectivity increases in the following order: CEM Type-I \cong MA-41 < AEM Type-I < MK-40 < CMX \cong CEM Type-II \cong CEM Type-X \cong AEM Type-II < AMX < AEM Type-X. It is shown that the properties of the AEM Type-I and CEM Type-I membranes are close to those of the heterogeneous MA-41 and MK-40 membranes, while the properties of Fujifilm Type-II and Type-X membranes are close to those of the homogeneous AMX and CMX membranes. This difference is related to the fact that the Type-I membranes have a relatively high parameter f_2 , the volume fraction of the electroneutral solution filling the intergel spaces. This high value is apparently due to the open-ended pores, formed by the reinforcing fabric filaments of the Type-I membranes, which protrude above the surface of these membranes.

Keywords: ion exchange membrane; electrospinning; electric conductivity; diffusion permeability; selectivity

1. Introduction

In recent years, the fields of application of electro dialysis (ED), dialysis, and other processes with ion-exchange membranes (IEM) have expanded rapidly. In these fields, the environmentally friendly membrane technologies actively replace traditional chemical and physico-chemical methods of purification, concentration, conditioning, and separation of substances [1–3]. These applications include wastewater treatment [4], the extraction of antioxidants from wine-making waste or the increase in their concentration in fruit juices [5], as well as the recovery of dietary supplements and valuable medicinal products from wastes of agricultural products processing [6,7].

It is known that IEMs are the most expensive part of ED devices. Their contribution to the total cost of the process can reach 40–50% [8]. Therefore, the degree of implementation of technologies that use ion-exchange membranes is generally determined by IEM transport properties and cost.

Until recently, the structure of membranes mainly used in commercial applications could be reduced to two main types: (1) homogeneous at the nanoscale level (up to 100 nm) single-phase IEMs (Nafion, DuPont Co., Wilmington, CA, USA; MF-4SK, JSC NPO Plastpolymer, Saint Petersburg, Russia; and others) or two-phase IEMs (Neosepta AMX, CMX, Astom, Tokyo, Japan; CJMC-3, CJMA-7, Hefei ChemJoy Polymer Materials, Hefei, China; and others), which are traditionally called “homogeneous”; and (2) heterogeneous IEMs, which consist of micrometer (from 5 to 50 microns) ion-exchange polymer granules incorporated into an inert binder (MK-40, MA-40, Shchekinoazot, Russia; Ralex MH-PES, MEGA a.s., Czech Republic; FTAM-E, FTAM-A, FuMA-Tech GmbH, Ludwigsburg, Germany) [1,9,10].

To increase the mechanical strength of IEM, they are usually reinforced with nets or fabrics made of various polymers (capron, polyester, polyvinyl chloride, etc.). Several years ago, in the framework of the European project “Blue Energy”, Fujifilm (the Netherlands) set up an industrial production of fundamentally new IEMs [11,12]. The basis of these membranes is a three-dimensional structure of nanofibers made using the electrospinning method [13,14]. We denote these membranes by the term “electro-spun nanofiber ion exchange membranes”, EN-IEMs. These fibers, whose diameter ranges from 40 nm to 25 μm , simultaneously play the role of an inert filler and a reinforcing material. The space between the fibers is filled with a homogeneous ion-exchange aliphatic polymer. Note that the original ion-exchange membranes manufactured using the electrospinning method were used to produce electricity by the reverse electro dialysis method. An overview of these works can be found in [15–17]. The developers mainly sought to provide low electrical resistance while maintaining the high mechanical strength of the new membranes. Recently, a number of attempts have been made to apply EN-IEMs in fuel cells [18], to obtain ultrapure water [19], to remove fluoride and arsenic ions from natural waters [20], and others.

Especially attractive is their use in the processing of liquid media of the food and pharmaceutical industries, where the main priorities are the energy costs, the ability of membranes to transfer not only small mineral ions (Na^+ , Cl^-), but also high-molecular compounds (polyphenols, amino acids, peptides, polysaccharides, and others), as well as their resistance to fouling by aromatic compounds [21–23]. However, the widespread introduction of relatively cheap membranes of this type is hampered by the lack of knowledge about transport characteristics of membranes manufactured by Fujifilm or experimental membranes, which have a similar structure [24,25]. To the best of our knowledge, the existing research is mainly devoted to the study of electric conductivity [26,27], the search for methods of the EN-IEM surface modification to control sedimentation [28], or to increase their specific selectivity to a specific type of counter-ions [29–31].

For example, in studies [26,27] it was shown that the electric conductivity of these membranes increases with an increase in their exchange capacity and decreases with an increase in the ionic strength of the external solution. The authors explain the last effect [27] by narrowing the conductive channels as a result of a decrease in the water content of the membranes.

The purpose of current work is a comprehensive study of the structural and transport characteristics (electric conductivity, diffusion permeability, transport numbers of co-ions and counterions) of three cation-exchange and three anion-exchange membranes manufactured by Fujifilm using the method of electrospinning. We will compare these data with the characteristics of known homogeneous and heterogeneous membranes and assess the prospects for using EN-IEMs in dialysis and electro dialysis processes.

2. Objects and Methods of Study

2.1. Membranes

Anion-exchange (AEM Type-I, AEM Type-II, AEM Type-X) and cation-exchange (CEM Type-I, CEM Type-II, CEM Type-X) membranes manufactured by Fujifilm (Tilburg, The Netherlands) were studied. The Fujifilm homogeneous membranes are based on a three-dimensional structure (substrate) of inert polyolefin fibers [12], which were obtained by electrospinning method [14]. The formation of fine fibers is carried out from a polymer solution in an organic solvent under the action of electric field of high strength. This solution is fed from the capillary needle and is accompanied by evaporation of the solvent. The thickness of the fibers is varied using different concentrations of polymer, the solution feed rate and the electric field strength [32–34]. The aerogel formed by the fibers is pressed to a predetermined thickness. The space between the fibers is filled with aliphatic polyamide, PA [23,26,35] functionalized by quaternary ammonium bases, $-(\text{CH}_3)_3\text{N}^+$, in the case of anion-exchange membranes (AEMs) [36] or sulfo groups, $-\text{SO}_3^-$, in the case of cation-exchange membranes (CEMs) [36]. The chemical structure of cation-exchange and anion-exchange EN-IEM is shown in Figure 1.

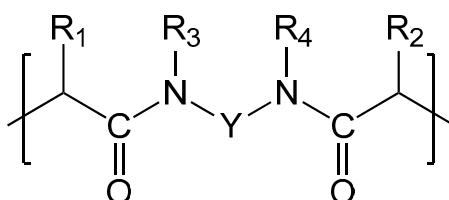


Figure 1. Chemical structure of cation- and anion-exchange EN-IEMs: R_1 and R_2 are each independently H or methyl; R_3 and R_4 are each independently H or alkyl, or R_3 and R_4 together with the N atoms to which they are attached, and Y form an optionally substituted 6- or 7-membered ring; Y is an optionally substituted and optionally interrupted alkylene or arylene group; provided that the structural unit has 1, 2, 3, or 4 sulfonic acid (CEM) or quaternary ammonium (AEM) groups.

Homogenous membranes AMX and CMX (produced by Astom, Tokuyama Soda, Japan) are made by the “paste method” [37,38]. Initially, the paste contains styrene monomer with functional groups (which are subsequently grafted with ion-exchange groups), divinylbenzene (45–65%) as a crosslinking agent, a radical polymerization initiator and powdered polyvinyl chloride (45–55%). The paste is deposited on the reinforcing polyvinyl chloride fabric. The copolymerization is carried out before the sulfonation (CEM) or amination (AEM). According to [39] such membranes consist of two interpenetrating phases: ion exchange material and polyvinyl chloride, PVC, having a particle diameter of 100 nm or less. The structural inhomogeneities in the membrane volume does not exceed 1 micron [40]. An exception is the reinforcing fabric having fibers of 25–30 μm in diameter.

Heterogeneous membranes MA-41 and MK-40 (manufactured by JSC Shchekinoazot) are made by hot rolling of low-pressure polyethylene, PE (used as a binder), with AV-17 and KU-2 ion-exchange resin powders, respectively. The size of polyethylene and ion-exchange resin particles is in the range from 5 to 50 microns. Reinforcing nylon mesh (where the diameter of filaments is of 30–50 microns) is introduced by hot pressing [41].

Summation of basic materials and membrane manufacturing methods are presented in Table 1. Some of the characteristics of the swollen membranes are presented in Table 2.

Table 1. Summation of basic materials and membrane manufacturing methods.

Membranes	Type	Ion Exchange Matrix	Fixed Groups	Inert Binder	Reinforcing Material	Manufacturing Method	
MA-41 MK-40	heterogeneous	DVB + PS	*	PE	nylon mesh	hot rolling	
			**				
AMX CMX	homogeneous	PA	*	PVC	PVC fabric	“paste” method	
			**				
AEM Type-I, AEM Type-II, AEM Type-X				*	-	3D polyolefin fibers structure	filling the voids of the 3D fiber structure with ion-exchange material
CEM Type-I, CEM Type-II, CEM Type-X				**			

* Mainly quaternary ammonium bases, $-(\text{CH}_3)_3\text{N}^+$, and a small amount of secondary and tertiary amines. ** Sulfo group $-\text{SO}_3^-$. DVB + PS is a copolymer of polystyrene and divinylbenzene; PE is low-pressure polyethylene; PA is polyamide; PVC is polyvinyl chloride.

Table 2. Some of the characteristics of the membranes under study. Our data are given without reference.

Membranes	Thickness of Air-Dried Membrane, Microns	* Thickness of Wet Membrane, Microns	Exchange Capacity, mmol g ⁻¹ wet	Density, g cm ⁻³ wet	Water Content, g H ₂ O/g wet, %	Water Content, mol H ₂ O/mol Functional Groups
Cation-Exchange						
CEM Type-I	120 ± 5 115 [42]	140 ± 10	1.43 ± 0.05	1.15	29 ± 5	11.3 ± 1
CEM Type-II	165 ± 5	180 ± 10 179 [43]	1.35 ± 0.05	1.13	25 ± 2	10.3 ± 1
CEM Type-X	125 ± 5 125 [42]	130 ± 5	1.67 ± 0.05	1.20	21 ± 5	7 ± 1
CMX	155 ± 5 155 [42]	170 ± 5	1.61 ± 0.05	1.32	22 ± 3	8 ± 1 (7.5)
		175 ± 6 [44]	1.65 ± 0.05 [46]	1.19 [48]	19 [50]	7.62 [52,53]
		163 [45]	1.62 ± 0.04 [31,47]	1.26 [49]	23 [51]	9 [54]
MK-40	440 ± 10	520 ± 20	1.43 ± 0.08	1.18	26 ± 5	10 ± 1
		520 ± 10 [55]	1.52 ± 0.08 [55]	1.13 [48]	34.7 [56]	12.1 ± 1
			1.69 [48]	1.19 [55]	33 ± 1 [55]	11.8 [57]
Anion-Exchange						
AEM Type-I	120 ± 5 115 [42]	125 ± 5	1.50 ± 0.05	1.06	8 ± 2	3.3 ± 1
AEM Type-II	165 ± 5 130 [19]	175 ± 5 175 [43]	1.08 ± 0.05	1.06	10 ± 5	5.5 ± 1
AEM Type-X	115 ± 5 125 [42]	120 ± 5	1.50 ± 0.05	1.08	23 ± 2	8.7 ± 1
AMX	125 ± 5	135 ± 5	1.23 ± 0.05	1.22	14 ± 2	6.5 ± 1
		141 ± 6 [23]	1.25 [47]	1.10 [58]	16 [50]	6.1 [23] 7.8 [54]
MA-41	430 ± 10	450 ± 50	1.22 ± 0.06	1.06	30 ± 2	8.7 ± 1
		530 ± 20 [55]	1.18 ± 0.06 [55]	1.14 [59]	30 [56]	13 [56]
			1.25 [46]		35 ± 2 [55]	7.1 [23]

* Membrane equilibrated with 0.02 M NaCl solution.

2.2. Reagents

In experiments we use: distilled water (electric conductivity of $1.1 \pm 0.1 \mu\text{S cm}^{-1}$; pH = 5.5; 25 °C), solid NaCl of the analytical grade (JSC Vecton), as well as natural dye—anthocyanin (Frutarom Etol d.o.o., Škofja Vas, Slovenia).

2.3. Methods of Membrane Characterization

Before conducting measurements, all membrane samples underwent standard salt preparation in NaCl solutions [9].

The total exchange capacity (Q_{sw}) is determined by the static acid-basic method [60], described in detail in Supplementary Materials.

Water content (W , %) of the membranes is determined as the mass ratio of water to swollen (sw) membrane by the gravimetric method, described in detail in Supplementary Materials.

The specific water-absorbing capacity (the number of moles of water per one mole of the fixed groups of the swollen membrane, n_w) was determined by the formula:

$$n_w = \frac{W}{P_{H_2O} \cdot Q} \quad (1)$$

where P_{H_2O} is the molar mass of water, equal to 18 g/mol; Q is the membrane exchange capacity, mol/g_w.

The thickness of the swollen membrane (d , μm) was controlled by a high-precision digital micrometer MKC-25 0.001 with an accuracy of 1 μm and with an error of 0.1 μm . The membrane thickness was obtained by averaging the results of 10 measurements made at various points of the sample under study.

The water contact angles of the swollen membrane surface were determined by the method of a resting drop described in [61]. The distilled water served as a test liquid. The water contact angles were recorded in 20 s after the test drop touches the rough surface of the membranes.

Visualization of the surface and volume of swollen IEM was carried out using an SOPTOP CX40M optical microscope (China) equipped with a digital eyepiece USB camera (5 \times , 10 \times , 20 \times , and 50 \times magnification). In order to increase the image contrast, Fujifilm membranes were placed in a solution containing a high molecular weight dye (anthocyanin) for 24 h before the measurements.

The morphology and chemical composition of the air-dry IEM surface was studied using the AFM method in “contact” mode (JEOL 5400 microscope, Tokyo, Japan, JEOL 5400 software), as well as using a scanning electron microscope (MERLIN™, Carl Zeiss Microscopy GmbH, Jena, Germany) equipped with an energy dispersive spectrometer (accelerating voltage is 6 kV, working distance is 9.9 mm) and the device for X-ray fluorescence elemental spectroscopy (XRF). To improve the contrast of the obtained images and reduce the electric field strength, a thin layer of platinum nanoparticles was sprayed onto air-dry membrane samples. The method of surface metallization is generally accepted for SEM studies of ion-exchange materials [62]. It is known that nanoparticles of platinum and gold have the smallest size compared with other metals [63]. Therefore, the use of these nanoparticles practically does not distort the geometry of the surface under study. To estimate the fractions of secondary and tertiary amines in the composition of fixed groups of anion-exchange membranes, the ability of weakly basic amines to form chemically strong complex compounds with copper(II) ions was used [64]. To this end, before obtaining XRF, the samples were pretreated with a 2 M CuSO₄ solution (pH = 4) for 48 h. Then samples were washed in distilled water to clean off the copper that did not enter the complex compounds. Studies of the structure and chemical composition were carried out on at least five different areas of each of the samples in order to ensure the reproducibility of the measurements. Dispersion in determining the elemental composition of membranes was ± 1 weight percent.

The specific electric conductivity of IEM (κ^*) was determined by a differential method using a clip cell [65,66] and an immittance meter MOTECH MT4080 (Motech Industries Inc., Taiwan) at an

alternating current frequency of 1 kHz. All samples were studied in 0.02–1.0 M NaCl solutions, starting from the lowest concentration.

The electric conductivity of membranes (κ^*) was determined by the equation:

$$\kappa^* = \frac{d_m}{R_{m+s} - R_s} \quad (2)$$

where R_{m+s} is the resistance of membrane and solution; R_s is the resistance of solution; and d_m is the membrane thickness in the solution of given concentration.

The diffusion characteristics of the IEM were investigated using a two-chamber flow cell [67]. The membrane separated two tracts: distilled water was pumped through one of them (tract I), and a NaCl solution of a given concentration was pumped through the other tract (II). Before the experiments, all samples were equilibrated with 0.02 M NaCl solution. The first measurements were carried out for the concentration of NaCl solution in tract II equal to 0.02 M. Then, this concentration was sequentially increased to 1.0 M. The membrane under investigation was in contact with each of the solutions for at least 5 h. The cell scheme, the methodology for conducting the experiment and processing the obtained data are described in detail in [68]. The error of determining the integral diffusion permeability coefficient, P , of membranes is equal to $\pm 0.4 \times 10^{-8} \text{ cm}^2\text{s}^{-1}$.

The transport numbers of counterions (t_1^*) and co-ions (t_A^*) in the membranes under study were obtained using the concentration dependences of the specific conductivity (κ^*) and the integral diffusion permeability coefficient of the membranes (P). The method of their determination and formulas for the calculation are presented in [69]:

$$t_1^* = \frac{1}{2} + \sqrt{\frac{1}{4} - \frac{P^*F^2c}{2RT\kappa^*}} \quad (3)$$

$$t_A^* = 1 - t_1^* \quad (4)$$

where F is the Faraday constant; R is the gas constant, T is the temperature; C is the electrolyte concentration (NaCl), P^* is the local diffusion permeability coefficient of the membrane, which is connected to integral diffusion permeability coefficient by the relation:

$$P^* = P + C \frac{dP}{dC} \quad (5)$$

The value of the local diffusion permeability coefficient was determined taking into account Equation (1) as [70]:

$$P^* = P(\beta + 1) \quad (6)$$

The coefficient $\beta = dl_gP/dl_gc$ was found as the slope of the concentration dependence of the integral diffusion permeability coefficient, presented in logarithmic coordinates. In accordance with the generally accepted definition [71], the values of the counterion transport numbers through the IEM give an idea of the membranes' selectivity.

The standard contact porosimetry was used to estimate the integral volume of sorbed water (V) and the number of water molecules per AEM fixed group as functions of the effective pore radius (r). This method is described in detail in the works [72,73]. The essence of the method consists in measuring the equilibrium curve of the integral volume of sorbed water (or other liquid) of the sample under investigation, which is clamped between two reference porous samples with a known pore distribution. Porometric curves for reference samples are obtained in independent experiments, for example, using the method of mercury porosimetry. A controlled change in the water content of the samples is carried out by evaporation.

The effective pore radii that dominate in the membrane under study were determined from the values recorded at the inflection points of the porogram presented in the coordinates $V-r$. The total water content in the pores of this and a smaller diameter was estimated by the values of V , in the areas of the plateau of the porograms that follow the inflection points. The total water content in

the test sample (V_0) was found by the difference in weight of the completely swollen and absolutely dry membranes.

3. Results and Discussions

3.1. Structural Characteristics of the Investigated Membranes

Figures 2 and 3 show the SEM and AFM images of the EN-IEM air-dry samples under study. The points in Figure 2 indicate where the elemental composition of the surface was determined using XRF. Optical images of swollen AMX Type I and MA-41 membrane samples are presented in Figures 4 and 5. Optical images of dry AMX Type I, AMX Type II, CMX Type I, and CMX Type II membrane samples are presented in Figure S1 in the Supplementary Materials. The randomly arranged reinforcing fibers of thickness from 10 to 25 microns occupy a significant part of the EN-IEM volume. Some of them protrude slightly above the surface. Cracks of elongated shape, apparently, are formed during drying of the samples before the SEM.

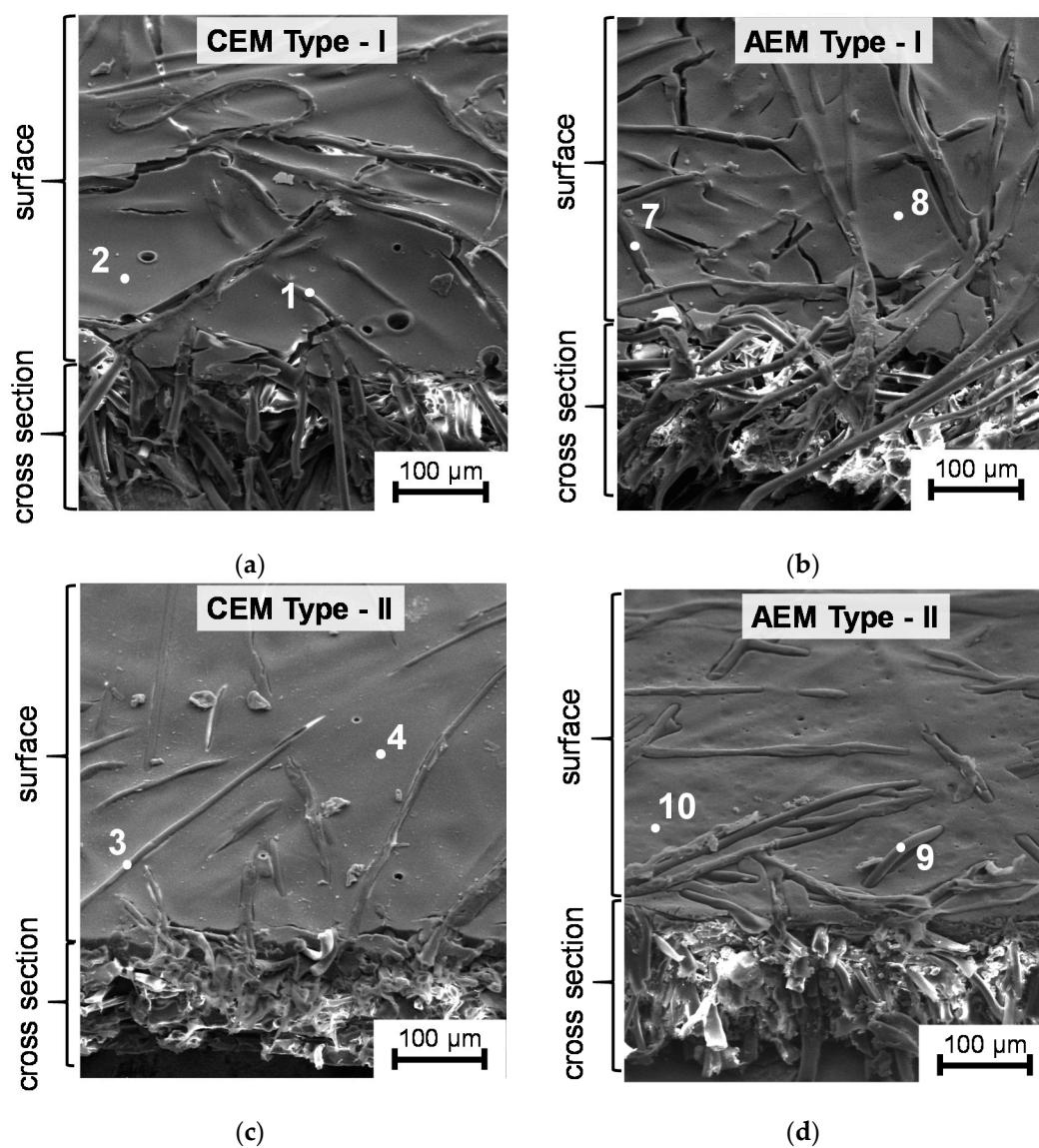


Figure 2. Cont.

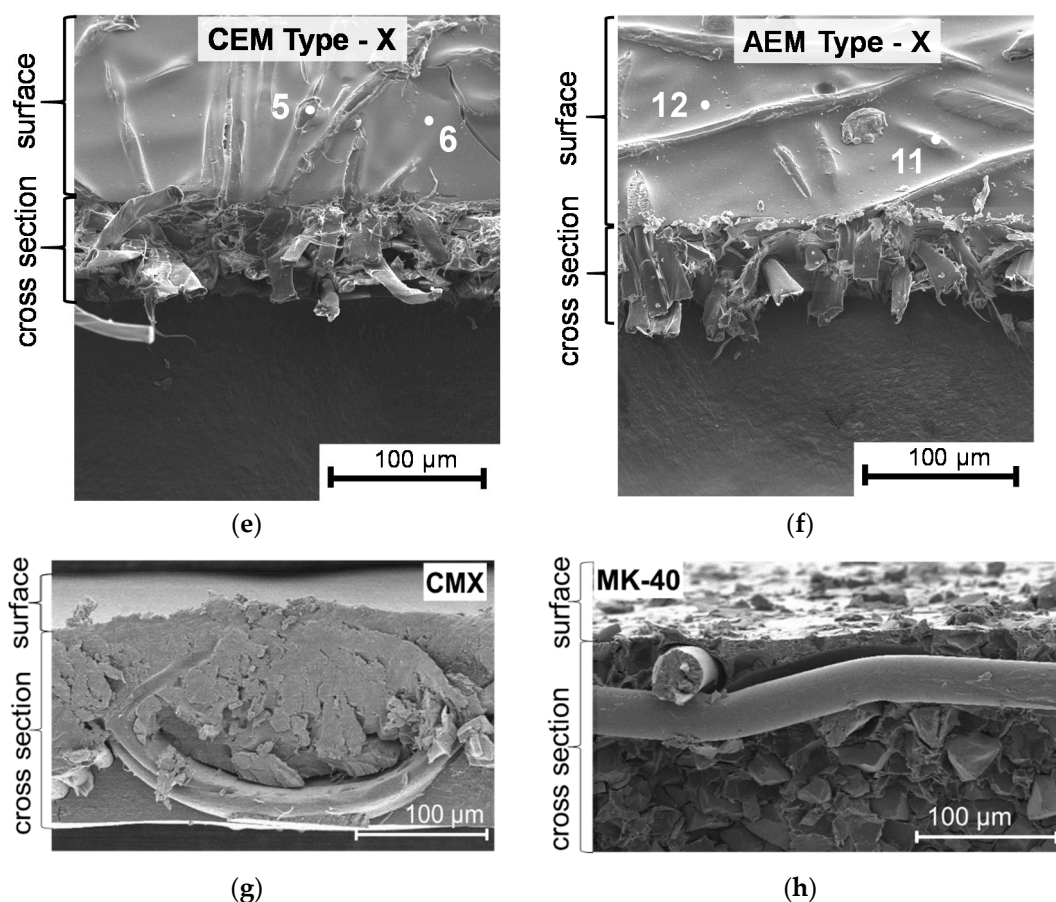


Figure 2. SEM images of the surface and cross sections of cation-exchange (a,c,e) and anion-exchange (b,d,f) IEM, manufactured using the electrospinning method, as well as Neosepta CMX (g) and heterogeneous MK-40 (h) membranes. The places where the element analysis was performed using the XRF are marked with white points.

In the SEM (Figure 2) and AFM (Figure 3) images of the EN-IEM surfaces, round holes are observed. The diameter of these holes varies from 3 to 25 microns (Figure 3). AFM images show that the average depth (R_z) of these holes is about 100 nm. These holes are visible on the surface of all investigated membranes (Figure 2).

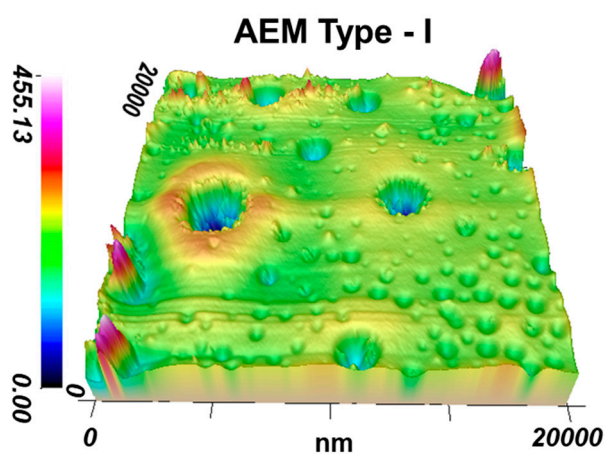


Figure 3. AFM image of air-dried sample of the AEM Type-I membrane.

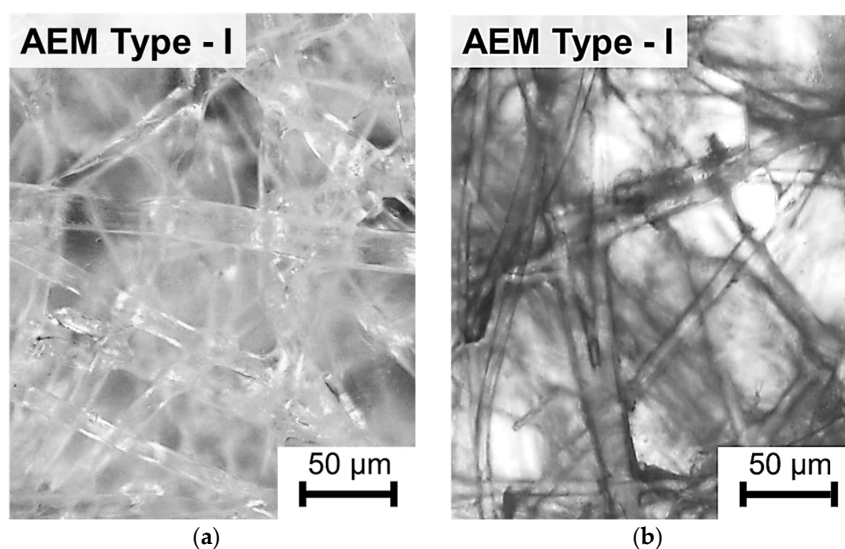


Figure 4. Optical images of the swollen AEM Type-I membrane. Before the study, samples were soaked in 0.02 M NaCl solution for 24 h (a) and in the 0.02 M NaCl solution where the high molecular weight dye (anthocyanin) was added (b).

The largest number of holes per surface unit is observed on the AEM Type I, CEM Type I, and CEM Type II membranes. Similar holes were found on membranes of this type by Y. Zhu et al. [35], who suggested that these holes are formed at the stage of membrane manufacturing, and their presence causes the deterioration of the transport characteristics of EN-IEMs. However, it is seen in the AFM (Figure 3) and SEM (Figure 2) images that most of these defects have a small depth (about 50–200 nm) and only some of them have a depth greater than 20 μm . Therefore, a noticeable effect of these holes on the transport properties of EN-IEMs seems unlikely. Optical microscopy data (Figure 4) allows one to conclude that extended (lengthy) macropores in some samples of EN-IEM (Type-I, Type-II) do exist, but they are formed at the interface of the polymer fiber with the ion-exchange material. In the case of swollen samples in equilibrium with sodium chloride solution, these pores are filled with an optically transparent equilibrium solution (Figure 4a).

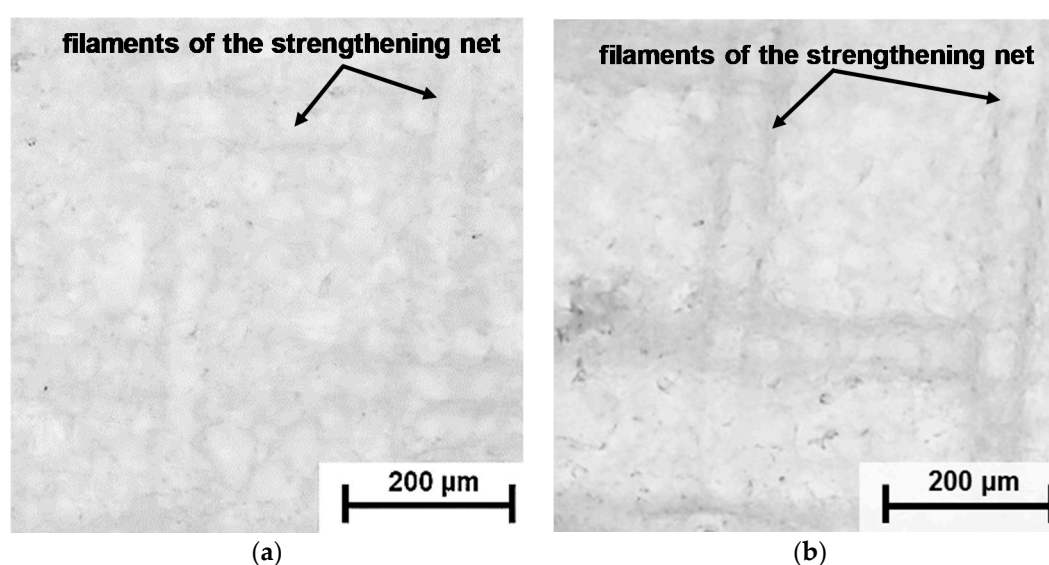


Figure 5. Cont.

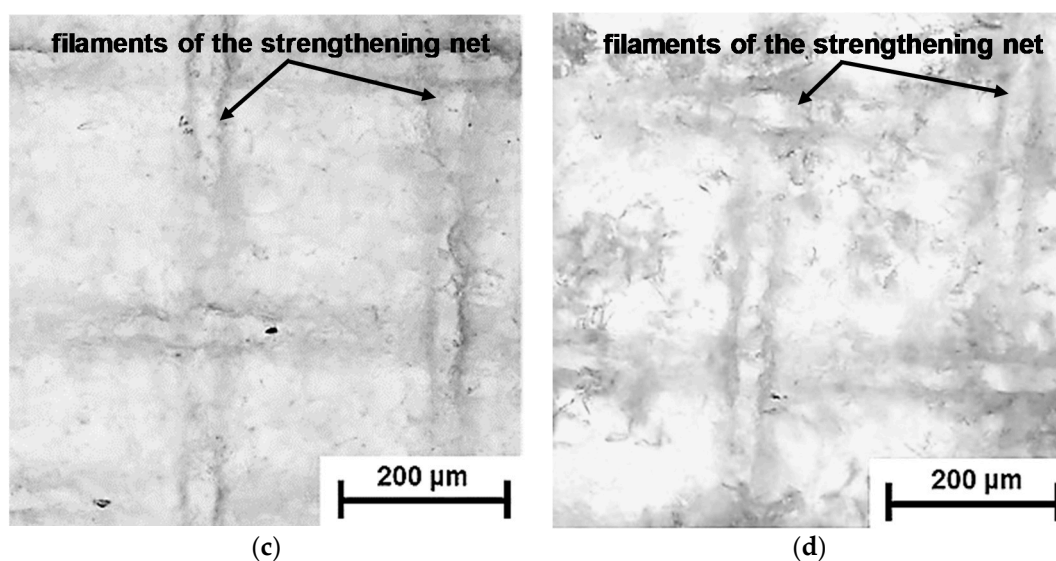


Figure 5. Optical images of the MA-41 membrane surface obtained using transmitted light mode in moments of time 10 s (a), 350 s (b), 720 s (c), and 900 s (d) after the beginning of contact of the swollen sample with the air.

After the contact of EN-IEM samples with a solution that contains a high molecular weight dye, its molecules do not penetrate into the microporous ion-exchange material, but transfer through large pores and are visualized as dark bands recorded at the interface between the fibers and ion-exchange material, as in the case of AEM Type-I shown in Figure 4b. Similar dark bands appear around the fibers in the swollen AEM Type-II membrane (Figure S2, Supplementary Materials).

The occurrence of diffusion pathways along the filaments of reinforcing net of swollen heterogeneous membranes can be observed although in the process of moisture evaporation from these membranes, as in the case of MA-41 membrane, Figure 5. Water has a higher optical density than air. Therefore, the near-surface membrane areas, where water is partly evaporated, should have a darker color. On the surface of a sample, which was in contact with air for a short time (Figure 5a), there are no dark areas. However, they appear after a few hundred seconds, especially at the intersections of the filaments of the reinforcing net, which are closest to the surface (Figure 5b). Then the dark areas spread along the entire length of the reinforcing net filaments and are localized at the borders between the filaments and other membrane components, ion-exchange resin particles, and polyethylene binder (Figure 5c), as well as at the boundaries between the resin particles and polyethylene binder in places where these particles reach the surface (Figure 5c). It is important to note that in the case of drying of homogeneous AMX and CMX membranes, such pores are not visualized.

The results obtained using standard contact porosimetry method show that the nanoporous structure of the MK-40 and MA-41 membranes is similar to that of the homogeneous membranes produced by the paste method (CMX, AMX). However, the MK-40 and MA-41 membranes have macropores with a radius of more than 35 nm, while the homogeneous membranes do not have such pores (Figure 6).

Indeed, in the range of effective pore radii from 1 to 15 nm, the porometric curves for heterogeneous (MA-41) and homogeneous (AMX) membranes are almost identical. The dominant effective pore radii, which correspond to the inflection points in the curves, are 3 and 13 nm. Such pore sizes are typical for homogeneous ion-exchange materials [73]. A similarity in porometric curves is explained by the fact that both membranes are made of styrene copolymer with divinylbenzene and have the same fixed groups. The dry MA-41 membrane is characterized by a higher concentration of fixed groups (exchange capacity), so water content in its micropores ($r < 3$ nm) and mesopores ($r < 13$ nm) is higher as compared to AMX. Both membranes have pores with a radius of about 35 nm, which, apparently, can be attributed to defects in the structure of ion-exchange polymers, but their contribution to the

total water content is insignificant, especially in the case of AMX. Further, the AMX porometric curve comes to a plateau, and the MA-41 porometric curve still has at least two inflections which indicate the presence of larger pores. The first of them (the effective radius is about 100–150 nm) could be attributed to macropores formed at the places of contact of resin particles with an inert reinforcing binder (polyethylene). Such pores were found, for example, in the images of the surface of swollen MK-40 and MA-41 membranes, using the low-vacuum SEM method [55].

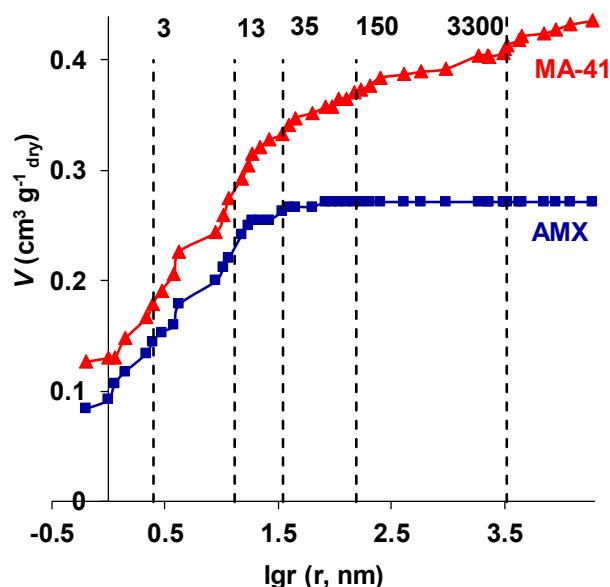


Figure 6. The dependence of the volume of sorbed water (V) on the effective pore radius (r) in an AMX and a MA-41 membrane. The vertical dashed lines indicate the inflection points on the curves; these points correspond to the radii of the pores whose fraction in the membranes is relatively high. The values (in nanometers) of these radii are shown by the numbers near the dashed lines.

The larger pores (>3000 nm) can be visualized by the optical method as dark areas (Figure 5). They are formed between the nylon reinforcing net and the resin particles as well as the polyethylene binder (Figure 5). According to our estimates, made by the analysis of porometric curves (Figure 6), both types of macropores (>100 nm) contain up to 25% of the water in MK-40 and MA-41 membranes. These voids appear when the membrane is dried. In the swollen state, the volume fraction of macropores may be evaluated as about 10% [74]. The absence of such large pores appearing when drying in homogeneous AMX (Figure 6) and CMX membranes is apparently associated with stronger adhesion of the reinforcing net and inert binder, which are produced from the same material, polyvinyl chloride.

The elemental composition of the investigated EN-IEMs is obtained using XRF and presented in Table 3. The reinforcing fibers and ion-exchange material are studied separately. In the case of fibers (the lines in Table 3 are indicated by odd numbers), the composition corresponds to polyolefin; in the case of ion-exchange material (indicated by even numbers), to polyamide (Figure 1), from which the membranes are made [36]. The sulfonic fixed groups of the CEM contain sulfur. The studied samples were in the H^+ form. These counterions are not identified by XRF. The presence of fixed amino groups in AEM leads to an increase in nitrogen concentration as compared to CEM.

Chlorine, which is found on the surface of AEM, is due to Cl^- , a counterion. The percentage of nitrogen and chlorine (in AEMs), as well as sulfur (in CEMs), increases in proportion to the growth in the exchange capacity of dry membranes (Table 3). It should be noted that all manufacturers and most of the researchers indicate that the functional groups of the studied AEMs are quaternary amines. However, these membranes contain secondary and tertiary amines [75]. According to XRF data (Figure S3, Supplementary Materials), copper (ions Cu^{2+}), which is an indicator of the presence of weakly basic groups, is evenly distributed over the surface and volume of ion exchange materials

and its mass fraction in the case of unused AMX, MA-41, AEM Type-II and AEM Type-X does not exceed 1% (see Figure S1a in the Supplementary Materials for an AEM Type-X membrane). An exception is the AEM Type-I membrane, the mass fraction of copper which reaches 3% (Figure S1b, Supplementary Materials). It is known [76] that the thermal destruction and/or nucleophilic attack of quaternary amines with hydroxyl ions (which are always present in aqueous solutions) is the cause of the secondary and tertiary amines formation. The transformation of strongly basic amines into weakly basic ones can occur both at the manufacturing stage and during the storage of membranes in aqueous solutions. This is probably why the information on the content of these groups in anion-exchange membranes, for example, in AMX, differs significantly [31,75]. Given that all membranes, with the exception of AMX, are stored in a dry state, it can be assumed that the higher content in AEM Type-I of secondary and tertiary amines is due to the special conditions of its manufacture.

Table 3. The elemental composition (in weight percent) of EN-IEM and their exchange capacity in the air-dry state.

Membranes		Elemental Composition (%)					Q , mmol g ⁻¹ dry
		Carbon (C1s)	Oxygen (O1s)	Nitrogen (N1s)	Chlorine (Cl2p)	Sulfur (S2p)	
Cation-Exchange Membranes							
CEM	* 1	99	1	-	-	-	2.02 ± 0.05
Type-I	2	54	26	11	-	9	
CEM	3	99	1	-	-	-	1.81 ± 0.05
Type-II	4	50	32	10	-	8	
CEM	5	100	-	-	-	-	2.12 ± 0.05
Type-X	6	52	27	8	-	13	
Anion-Exchange Membranes							
AEM	7	99	1	-	-	-	1.65 ± 0.05
Type-I	8	57	21	16	6	-	
AEM	9	99	1	-	-	-	1.21 ± 0.05
Type-II	10	63	19	14	4	-	
AEM	11	100	-	-	-	-	1.96 ± 0.05
Type-X	12	75	5	13	7	-	

* The number in the table corresponds to the number of the membrane area indicated in Figure 2 which was analyzed using XRF. Even numbers denote the ion exchange material, odd numbers denote the reinforcing fibers.

Thus, both the studied heterogeneous membranes and EN-IEMs contain extended macropores, which are formed at the points of contact of the fibers (Type-I and Type-II) and the reinforcing net (MA-41, MK-40) with the ion-exchange material. There are no such pores in the AMX and CMX membranes.

In general, the chemical composition of the investigated membranes corresponds to that declared by the manufacturers. All CEM contain sulfonic functional groups. All AEM contain strongly basic quaternary amines. The AEM Type-I membrane is characterized by the greatest portion of weakly basic functional groups in comparison with other studied AEM.

3.2. Membrane Transport Characteristics

The specific conductivity of the membranes. Figures 7a and 8a show the concentration dependences of the specific conductivity of the investigated membranes in sodium chloride solutions. In Figures 7b and 8b the dependences of the specific conductivity of these membranes on the specific conductivity of NaCl solutions with which these membranes are equilibrated are shown in logarithmic coordinates. Such data processing allows determining the volume fractions of the gel phase (f_1) and the phase of the electroneutral solution filling the intergel spaces (f_2) of the investigated membranes according to the microheterogeneous model [59]. This model, in the simplest case, considers an IEM

as a two-phase system. The gel phase is a microporous swollen medium, which includes a polymer matrix that carries fixed charged groups, as well as a charged solution of mobile counterions (and the co-ions in a smaller amount), which compensates the charge of fixed groups. The reinforcing fibers (fabric), inert filler or binder are considered as parts of the polymer matrix. The electroneutral solution filling the intergel spaces, which are the central part of the mesopores and the structural defects of the membrane, is assumed identical to the external solution.

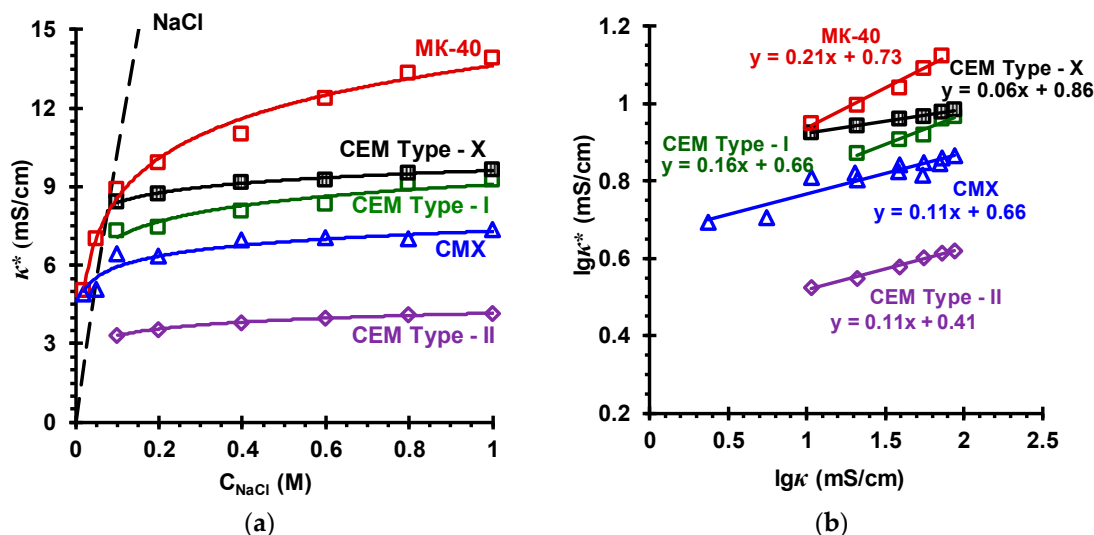


Figure 7. Concentration dependences of the conductivity of different cation-exchange membranes, κ^* , in NaCl solutions (a) and the $lg\kappa^*$ vs. $lg\kappa$ dependences of these membranes in NaCl solutions (b). The names of the membranes are indicated near the curves, which fit the experimental data. The dashed line in the figure (a) is the concentration dependence of the NaCl solution conductivity.

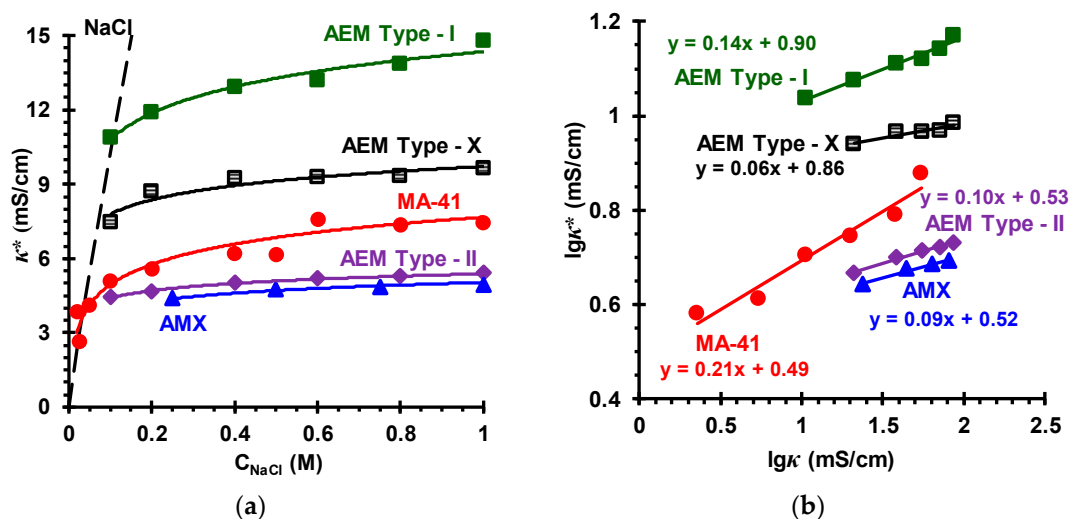


Figure 8. Concentration dependences of the conductivity of different anion-exchange membranes, κ^* , in NaCl solutions (a) and the $lg\kappa^*$ vs. $lg\kappa$ dependences of these membranes in NaCl solutions (b). The names of the membranes are indicated near the curves, which fit the experimental data. The dashed line in the figure (a) is the concentration dependence of the NaCl solution conductivity.

The simplified equation connecting the conductivity of the membrane (κ^*) with the conductivities of the gel phase ($\bar{\kappa}$) and the intergel solution (κ), in the framework of the microheterogeneous model, reads:

$$\kappa^* = \bar{\kappa}^{f_1} \kappa^{f_2} \tag{7}$$

According to Equation (7), the $\lg \kappa^*$ vs. $\lg \kappa$ dependence should be a straight line, the conductivity of the gel phase being considered as constant. The slope of this line is equal to f_2 ($f_1 + f_2 = 1$), the other coefficient of this linear dependence allows finding the value of $\bar{\kappa}$.

Knowing the value of $\bar{\kappa}$, it is possible to estimate the counterion diffusion coefficient, \bar{D}_1 , in the gel phase (when neglecting the contribution of co-ions to the conductivity):

$$\bar{D}_1 = (RT/F^2)(\bar{\kappa}/\bar{Q}) = (RT/F^2)(\bar{\kappa}f_1/Q) \quad (8)$$

Here R is the gas constant; T is the temperature; Q is the membrane exchange capacity (mmol cm^{-3} membrane), $\bar{Q} = Q/f_1$ is the exchange capacity of the gel phase of the swollen membrane (mmol cm^{-3} gel).

Note that the concentration at which the conductivities of the membrane, gel phase and external solution are equal is called the isoconductivity point, the corresponding concentration is denoted as C_{iso} . At concentrations less than C_{iso} (for studied IEM, C_{iso} is in the range of 0.03–0.10 M solutions), $\bar{\kappa}$ is greater than κ ; at $C > C_{\text{iso}}$, $\bar{\kappa}$ is lower than κ .

The values of f_2 , $\bar{\kappa}$, \bar{Q} , and \bar{D}_1 found as described above are presented in Table 4. In the case of studied membranes with an aromatic ion exchange matrix, these values are in good agreement with the literature data (Tables 2 and 4). Some differences, apparently, are due to the fact that the properties of all membranes vary from one surface site to another; they depend on the peculiarities of membrane preparation as well as the storage conditions.

Table 4. The values of conductivity at the isoconductivity points, volume fraction, exchange capacity of and counterion diffusion coefficient in the gel phase of the investigated membranes in NaCl solution.

Membranes	f_2	$\bar{\kappa}$, mS cm^{-1}	\bar{Q} , mmol cm^{-3} wet gel	$\bar{D}_1 10^{10}$, $\text{m}^2 \text{s}^{-1}$
Cation-Exchange Membranes				
CEM Type-I	0.16 ± 0.1	6.1 ± 0.1	1.65 ± 0.05	0.67
CEM Type-II	0.11 ± 0.01	2.8 ± 0.1	1.53 ± 0.05	0.36
CEM Type-X	0.06 ± 0.01	8.2 ± 0.1	2.01 ± 0.05	0.97
CMX	0.11 ± 0.03	5.5 ± 0.1	2.13 ± 0.05	0.63
	0.06 [57]	6.72 [57]		
	0.10 [46]	8.79 [46]		
MK-40	0.21 ± 0.03	8.3 ± 0.1	1.74 ± 0.05	0.88
	0.25 [46]	5.27 [57]		
	0.18 [57]	6.4 [56]		
	0.20 [56]			
Anion-Exchange Membranes				
AEM Type-I	0.14 ± 0.03	10.9 ± 0.1	1.60 ± 0.05	1.52
AEM Type-II	0.11 ± 0.02	3.9 ± 0.1	1.14 ± 0.05	0.76
AEM Type-X	0.06 ± 0.02	8.3 ± 0.1	1.63 ± 0.05	1.05
AMX	0.09 ± 0.03	3.7 ± 0.1	1.50 ± 0.05	0.62
	0.11 [46]	3.72 [46]		
		4.3 [77]		
MA-41	0.21 ± 0.03	4.2 ± 0.1	1.30 ± 0.05	0.58
	0.24 [46]	4.0 [46]		
	0.18 [57]	5.8 [57]		
		6.3 [56]		

The values of $\bar{\kappa}$ increase in the series CEM Type-II < MK-40 < CMX \approx CEM Type-I < CEM Type-X (for CEMs) and AMX \approx AEM Type-II < MA-41 < AEM Type-X < AEM Type-I (for AEMs) in the same order as the exchange capacity of the gel phase (Table 4).

An exception is the AEM Type I membrane. The values of $\bar{\kappa}$ and \bar{D}_1 for this membrane are greater as compared to AEM Type-X at close values of \bar{Q} for both membranes. This experimental fact is

probably explained by a higher content of secondary and tertiary amino groups in the AEM Type-I membrane (Figure S1, Supplementary Materials). Our studies show that the treatment of a weakly basic heterogeneous MA-40 membrane (JSC Shchekinazot, Russia) with a modifier, which leads to shielding of secondary and tertiary fixed amino groups with quaternary amines, causes a decrease in the conductivity of this membrane in 1 mol dm⁻³ NaCl solution from 6.9 to 4.5 mS cm⁻¹, while f_2 of the pristine and modified membranes do not change significantly [78].

As one would expect, in the moderately concentrated solutions (0.1 M < C < 1.0 M), the rate of increase in conductivity of all investigated membranes with respect to the conductivity at the C = C_{iso} is determined by f_2 : the higher this value, the stronger the conductivity increases with increasing concentration of the external solution.

Diffusion permeability of ion-exchange membranes. Figure 9 shows the concentration dependences of the integral diffusion permeability coefficient, P, of investigated membranes in NaCl solutions. It is known [71] that the value of P (or the value of differential diffusion permeability P*, Equation (5)) is mainly determined by the rate of co-ion diffusion, which depends on the gel phase exchange capacity (\bar{Q}), the co-ion concentration (\bar{C}_A) and diffusion coefficient (\bar{D}_A) in this phase, the volume fraction of electroneutral solution (f_2) and the relative disposition of the gel and intergel solution phases, parameter α [59]:

$$P^* = 2t_1^* [f_1(\bar{D}_A \bar{C}_A)^\alpha + f_2(D_A C)^\alpha]^{1/\alpha} RT/C \tag{9}$$

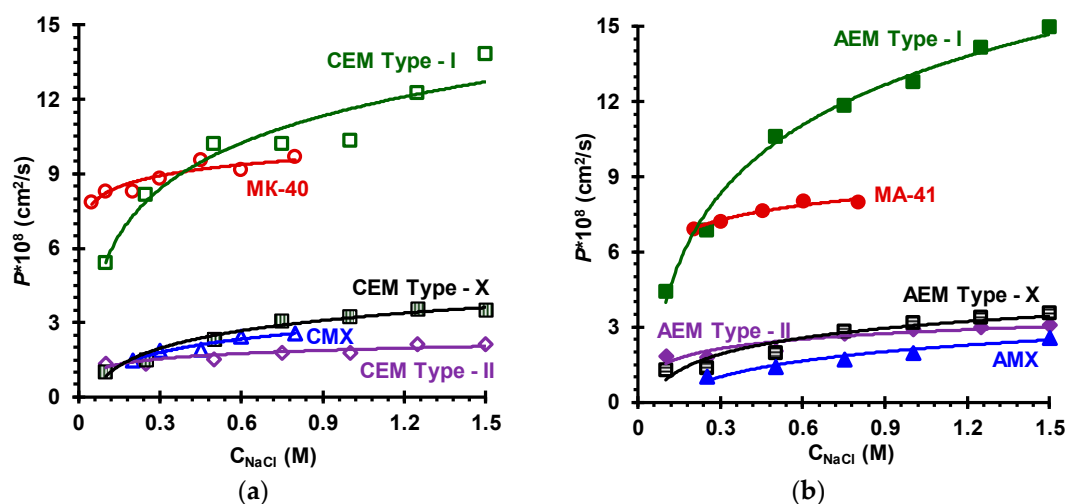


Figure 9. Concentration dependences of the integral diffusion permeability coefficient for cation-exchange (a) and anion-exchange membranes (b) in NaCl solutions.

The value of \bar{Q} determines the degree of electrostatic (Donnan) exclusion of co-ions from the gel phase and determine the value of the counterion transport number (t_1^*); f_2 determines the intergel solution regions where this electrostatic exclusion is absent. The greater \bar{Q} (t_1^*) and the lesser f_2 , the lesser the diffusion permeability of the membrane. The value of P increases when the gel and intergel solution phases are disposed so that the intergel solution forms a continuous pathway for co-ions, that is, the phases are mainly in parallel to each other (α approaches 1) and the contribution of the series disposition of phases is low. Dilution of the solution should lead to a decrease in the diffusion permeability of the membranes due to increase in electrostatic (Donnan) exclusion of co-ions from the gel phase [71].

The contribution of macropores to the membrane transport properties, in particular, to diffusion permeability, depends on the amount of these pores per unit volume and their disposition in space. These pores are mainly formed at the interfaces of different structure elements of the membrane, namely,

ion-exchange material, binder and reinforcing fabric. The highest volume fraction of macropores expressed by the highest value of f_2 is in the heterogeneous MK-40 and MA-41 membranes (about 0.2); the Type-I cation- and anion-exchange Fujifilm membranes have f_2 close to 0.15; the other studied membranes, Fujifilm and Neosepta, have this parameter between 0.06 and 0.11 (Table 4). The value of P is the lowest for the membranes with small f_2 , it is essentially higher for the MK-40, MA-41 and Type I cation- and anion-exchange Fujifilm membranes. However, it can be remarked that the values of P are close for the last four membranes, while f_2 is noticeably different. This can be explained by higher fraction of parallel disposition of macropores (higher α) in the Type I membranes in comparison with the MK-40 and MA-41 membranes. The reason for higher α could be in the appearance of long open-ended macropores along the fiber of the reinforcing, which protrude over the membrane surface. These pores form continuous pathways not interrupted by the elements of the gel phase, which is almost impermeable for co-ions. SEM images show that in the case of Type-I membranes (Figure 2a,b) there is a great number of protrusions of the reinforcing fibers over their surface. This hypothesis is supported by the literature data [35], claiming that the selectivity of the CEM Type-I membrane increases when the membrane surface on the receiving side is covered with a film of ion-selective material. The number of these protrusions is much lower in the case of heterogeneous MK-40 and MA-41 membrane (Figure 2h), where the filaments of the fabric are immersed into the membrane body. Similarly, the fibers of the reinforcing fabric are immersed within the Neosepta membranes (Figure 2g). In addition, there is a good adhesion between the reinforcing fabric and ion-exchange material of the Neosepta membranes due to the similarity of their chemical composition (see Section 2.1). As for the Type-II and Type-X of EN-IEMs, as Figure 2c–f show, the number of fibers and their protrusions on the surface is essentially lower than in the case of the Type I membranes.

Counterion and co-ion transport numbers. Figure 10 shows the concentration dependences of the (real) transport numbers (t_1^*) of counterions in the investigated IEMs, which are found from the values of their conductivity and diffusion permeability using the approach [69] described above in Section 2.3, Equation (3). Table 5 summarizes t_1^* , determined by the authors of this paper and by other researchers, as well as the apparent transport numbers (t_{1app}^*) from literature, determined using the potentiometric method [9,79]. As a rule, t_{1app}^* values are indicated in the catalogs of manufacturers.

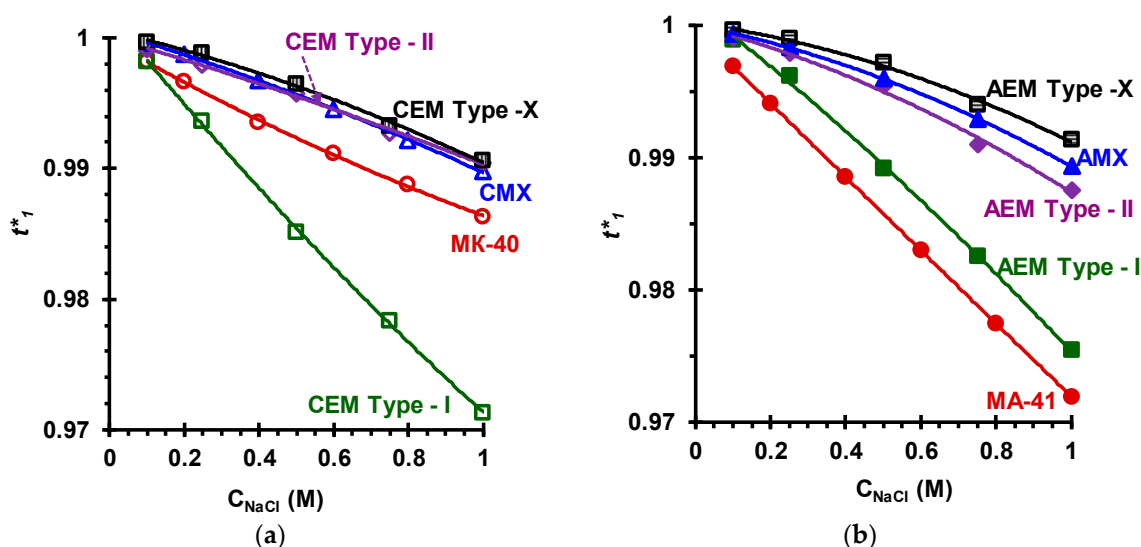


Figure 10. The concentration dependence of the real counterion transport numbers in the cation- (a) and anion-exchange (b) membranes.

The relationship between the real and apparent transport numbers is determined by the Scatchard equation [9,80]:

$$t_{1app}^* = t_1^* - z_1 n_1 m_s M_w t_w \tag{10}$$

where m_s is the molality of the solution, M_w is the molar mass of water, z_1 and n_1 are the charge and stoichiometric numbers of counterion, t_w is the water transport number showing how many moles of water are transported when 1 Farad of electric charge passes through the membrane.

Table 5. The values of real (t_1^*) and apparent (t_{1app}^*) counterion transport numbers, as well as the water transport number (t_w) in the membranes under study at solution concentration of 0.5 mol dm⁻³.

Membranes	t_1^*	t_{1app}^*	t_w
Cation-Exchange Membranes			
CEM Type-I	0.985	0.950 [12]	3.9
CEM Type-II	0.996	0.976 [12]	2.2
CEM Type-X	0.996	0.994 [12]	0.2
CMX	0.995	0.98 [81]	1.7
		0.965 [2] (NaCl)	
		0.94 [36]	5.8
MK-40	0.992	0.95 [82]	6.5 [56]
		0.965 [83] (KCl)	
Anion-Exchange Membranes			
AEM Type-I	0.989	0.950 [12]	4.3
AEM Type-II	0.995	0.970 [12]	2.8
AEM Type-X	0.997	0.970 [12]	3
AMX	0.996	0.98 [84]	1.9
			5.1
MA-41	0.986	0.950 [85]	5.0 [56]

The real (electromigration) ion transport number is a fundamental characteristic of the selective properties of ion-exchange membranes. The value of t_{1app}^* depends not only on the real transport number t_1^* , but also on the membrane electroosmotic permeability, which determines the value of t_w , Equation (10). The values of t_w , found using Equation (10) and known values of t_1^* and t_{1app}^* are presented in Table 5.

The determined values of the real counterion transport numbers in homogeneous (AMX, CMX) and heterogeneous (MA-41, MK-40) aromatic membranes are in good agreement with the results obtained by other researchers [69]. In the case of relatively concentrated solutions ($C = 1.0$ M), the permselectivity of the CEM Type-II and CEM Type-X cation-exchange membranes (Figure 10a) and the AEM Type-II and AEM Type-X anion-exchange membranes is close to that determined for the homogeneous CMX and AMX membranes (Astom, Japan) with an aromatic matrix. The permselectivity of the Type-I cation- and anion-exchange membranes is comparable to that of heterogeneous membranes MK-40, MA-41 (Shchekinoazot, Russia). In all cases, the co-ion transport numbers in the 1.0 M NaCl solution do not exceed the value of 0.03.

4. Conclusions

A comparative analysis of the concentration dependences of the conductivity, diffusion permeability, real and apparent ion transport numbers in cation- and anion-exchange membranes produced by three manufacturers was conducted. The microheterogeneous model [59] was applied to the interpretation of the experimental results.

The studied membranes involves (1) Neosepta AMX and CMX membranes (Astom, Japan), which are traditionally called homogeneous; (2) heterogeneous IEMs, which consist of micrometer (from 5 to 50 microns) ion-exchange resin particles, incorporated in an inert binder (MK-40, MA-40, JSC Shchekinoazot, Russia), and (3) Type-I, Type-II, and Type-X anion-exchange and cation-exchange membranes by Fujifilm, the Netherlands, which are based on a three-dimensional structure of interlaced fibers with a diameter from 40 nm to 25 μ m; the space between the fibers is filled with a homogeneous ion-exchange polymer. Membranes (1) and (2) contain ion exchange materials, which are based

on copolymers of polystyrene with divinylbenzene. They are reinforced with fabric (1) or net (2), made of polymeric materials. The basis of ion exchange membrane materials (3) is hydrophilic aliphatic polyamide. The three-dimensional structure of interwoven fibers simultaneously performs the functions of both a filler and a reinforcing material.

In NaCl solutions, all types of cation- and anion-exchange membranes manufactured by Fujifilm have a high permselectivity sufficient for use in electro dialysis of dilute solutions. The real counterion transport numbers in the Type-II and Type-X membranes are close to the values characteristic to CMX and AMX membranes, which are widely used in various electromembrane processes. In the Type-I membranes, transport numbers are similar to those determined in heterogeneous membranes MK-40 and MA-41.

The concentration dependences of the conductivity and diffusion permeability of Fujifilm membranes generally follow the same laws that are known for well-studied homogeneous (CMX, AMX) and heterogeneous (MK-40, MA-41) membranes. The structure-property relationships of all these membranes are well described and predicted by the microheterogeneous model.

One of the features in the behavior of Fujifilm membranes is in the fact the Type-I membranes show a high diffusion permeability and low permselectivity comparable to those of the heterogeneous MK-40 and MA-41 membranes. The reason, apparently, lies in the fact that the manufacturing of these membranes allows the formation of open-ended macropores on the membrane surface due to the protrusions of the fabric filaments above the surface. In the CMX and AMX membranes, large extended pores are practically absent, because the reinforcing fabric and filler of the ion exchange material are made of the same polymer (polyvinyl chloride) and have a good adhesion to each other.

In the case of MK-40, MA-41, the effect of these pores on the transport characteristics is essentially lower than in the case of the Type-I membranes, since the reinforcing net is immersed inside the membrane bulk.

Supplementary Materials: The following are available online at <http://www.mdpi.com/2077-0375/9/7/84/s1>, Figure S1: Optical images of air-dry AMX Type I (a), AMX Type II (b), CMX Type I (c), CMX Type II (d) membrane samples; Figure S2: Optical images of the swollen AEM Type-II membrane. Samples soaked in a 0.02 M NaCl solution for 24 hours (a), and the same samples in the 0.02 M NaCl solution where a high molecular weight dye (anthocyanin) is added (b); Figure S3: The distribution of Cu²⁺ ions in the composition of complexes with secondary and tertiary amines in the cross-sections of AEM Type-X (a) and AEM Type-I (b) membranes. The area mapped using XRF is 100×100 μm².

Author Contributions: Conceptualization: N.P. and V.N.; methodology: N.P.; formal analysis: C.L. and L.D.; investigation: V.S., S.M., C.L., and L.D.; resources: C.L. and L.D.; writing—original draft preparation: V.S.; writing—review and editing: C.L. and N.P.; experimentation: V.S., I.S., S.M., and N.K.; supervision: V.N. and N.P.; project administration: N.P.; funding acquisition: V.N. and V.S. All authors have approved the final article.

Funding: This research was funded by RSF grant number 19-19-00381 (investigation of CMX, AMX, MA-41, MK-40 membranes), and RFBR grant number 18-38-00521 mol_a (investigation of FujiFilm membranes). The authors thank the Core Facility “Environmental Analytical Center” of Kuban State University (unique identifier RFMEFI59317X0008) for providing their equipment.

Conflicts of Interest: The authors declare no conflict of interest.

References

1. Ran, J.; Wu, L.; He, Y.; Yang, Z.; Wang, Y.; Jiang, C.; Ge, L.; Bakangura, E.; Xu, T. Ion exchange membranes: New developments and applications. *J. Membr. Sci.* **2017**, *522*, 267–291. [[CrossRef](#)]
2. Calvo, E.J. Electrochemical methods for sustainable recovery of lithium from natural brines and battery recycling. *Curr. Opin. Electrochem.* **2019**, *15*, 102–108. [[CrossRef](#)]
3. Pawlowski, S.; Crespo, J.G.; Velizarov, S. Profiled ion exchange membranes: A comprehensible review. *Int. J. Mol. Sci.* **2019**, *20*, 165. [[CrossRef](#)]
4. Lee, S.; Choi, J.; Park, Y.-G.; Shon, H.; Ahn, C.H.; Kim, S.-H. Hybrid desalination processes for beneficial use of reverse osmosis brine: Current status and future prospects. *Desalination* **2019**, *104*, 104–111. [[CrossRef](#)]
5. Bazinet, L.; Doyen, A. Antioxidants, mechanisms, and recovery by membrane processes. *Crit. Rev. Food Sci. Nutr.* **2017**, *57*, 677–700. [[CrossRef](#)] [[PubMed](#)]

6. Kim, M.-S.; Na, J.-G.; Lee, M.-K.; Ryu, H.; Chang, Y.-K.; Triolo, J.M.; Yun, Y.-M.; Kim, D.-H. More value from food waste: Lactic acid and biogas recovery. *Water Res.* **2016**, *96*, 208–216. [CrossRef] [PubMed]
7. Xie, M.; Shon, H.K.; Gray, S.R.; Elimelech, M. Membrane-based processes for wastewater nutrient recovery: Technology, challenges, and future direction. *Water Res.* **2016**, *89*, 210–221. [CrossRef]
8. Mikhaylin, S.; Bazinet, L. Fouling on ion-exchange membranes: Classification, characterization and strategies of prevention and control. *Adv. Colloid Interface* **2016**, *229*, 34–56. [CrossRef]
9. Berezina, N.P.; Kononenko, N.A.; Dyomina, O.A.; Gnusin, N.P. Characterization of ion-exchange membrane materials: Properties vs. structure. *Adv. Colloid Interface* **2008**, *139*, 3–28. [CrossRef]
10. Xu, T. Ion exchange membranes: State of their development and perspective. *J. Membr. Sci.* **2005**, *263*, 1–9. [CrossRef]
11. Logan, B.E.; Elimelech, M. Membrane-based processes for sustainable power generation using water. *Nature* **2012**, *488*, 313–319. [CrossRef] [PubMed]
12. Ion Exchange Membranes for Water Purification. Brochure of Fujifilm Membrane Technology. Version Number 1.0. 2018. Available online: <https://www.fujifilmmembranes.com/water-membranes/ion-exchange-membranes> (accessed on 14 June 2019).
13. Cavaliere, S.; Subianto, S.; Savych, I.; Jones, D.J.; Rozière, J. Electrospinning: Designed architectures for energy conversion and storage devices. *Energy Environ. Sci.* **2011**, *4*, 4761–4785. [CrossRef]
14. University of Delaware. Method of Solution Preparation of Polyolefin Class Polymers for Electrospinning Processing Included. U.S. Patent B29C 47178, PCT/US2006/061206, WO 2007/062393 A2, 31 May 2007.
15. Tufa, R.A.; Curcio, E.; Van Baak, W.; Veerman, J.; Grasman, S.; Fontananova, E.; Di Profio, G. Potential of brackish water and brine for energy generation by salinity gradient power-reverse electro dialysis (SGPRE). *RSC Adv.* **2014**, *4*, 42617–42623. [CrossRef]
16. Vermaas, D.A.; Saakes, M.; Nijmeijer, K. Doubled power density from salinity gradients at reduced intermembrane distance. *Environ. Sci. Technol.* **2011**, *45*, 7089–7095. [CrossRef]
17. Tedesco, M.; Cipollina, A.; Tamburini, A.; Micale, G. Towards 1 kW power production in a reverse electro dialysis pilot plant with saline waters and concentrated brines. *J. Membr. Sci.* **2017**, *522*, 226–236. [CrossRef]
18. Tamura, T.; Kawakami, H. Aligned electrospun nanofiber composite membranes for fuel cell electrolytes. *Nano Lett.* **2010**, *10*, 1324–1328. [CrossRef]
19. Bhadja, V.; Makwana, B.S.; Maiti, S.; Sharma, S.; Chatterjee, U. Comparative efficacy study of different types of ion exchange membranes for production of ultrapure water via electrodeionization. *Ind. Eng. Chem. Res.* **2015**, *54*, 10974–10982. [CrossRef]
20. Bhadja, V.; Trivedi, J.S.; Chatterjee, U. Efficacy of polyethylene interpolymer membranes for fluoride and arsenic ion removal during desalination of water: Via electro dialysis. *RSC Adv.* **2016**, *6*, 67118–67126. [CrossRef]
21. Higa, M.; Tanaka, N.; Nagase, M.; Yutani, K.; Kameyama, T.; Takamura, K.; Kakihana, Y. Electro dialytic properties of aromatic and aliphatic type hydrocarbon-based anion-exchange membranes with various anion-exchange groups. *Polymer* **2014**, *55*, 3951–3960. [CrossRef]
22. Tanaka, N.; Nagase, M.; Higa, M. Organic fouling behavior of commercially available hydrocarbon-based anion-exchange membranes by various organic-fouling substances. *Desalination* **2012**, *296*, 81–86. [CrossRef]
23. Rijnaarts, T.; Moreno, J.; Saakes, M.; de Vos, W.M.; Nijmeijer, K. Role of anion exchange membrane fouling in reverse electro dialysis using natural feed waters. *Colloid Surf. A* **2019**, *560*, 198–204. [CrossRef]
24. Choi, J.; Lee, K.M.; Wycisk, R.; Pintauro, P.N.; Mather, P.T. Nanofiber network ion-exchange membranes. *Macromolecules* **2008**, *41*, 4569–4572. [CrossRef]
25. Park, A.M.; Turley, F.E.; Wycisk, R.J.; Pintauro, P.N. Electrospun and cross-linked nanofiber composite anion exchange membranes. *Macromolecules* **2013**, *47*, 227–235. [CrossRef]
26. Zhang, W.; Ma, J.; Wang, P.; Wang, Z.; Shi, F.; Liu, H. Investigations on the interfacial capacitance and the diffusion boundary layer thickness of ion exchange membrane using electrochemical impedance spectroscopy. *J. Membr. Sci.* **2016**, *502*, 37–47. [CrossRef]
27. Fontananova, E.; Messina, D.; Tufa, R.A.; Nicotera, I.; Kosma, V.; Curcio, E.; van Baak, W.; Drioli, E.; Di Profio, G. Effect of solution concentration and composition on the electrochemical properties of ion exchange membranes for energy conversion. *J. Power Sources* **2017**, *340*, 282–293. [CrossRef]

28. Liu, H.; Ruan, H.; Zhao, Y.; Pan, J.; Sotto, A.; Gao, C.; der Bruggen, B.V.; Shen, J. A facile avenue to modify polyelectrolyte multilayers on anion exchange membranes to enhance monovalent selectivity and durability simultaneously. *J. Membr. Sci.* **2017**, *543*, 310–318. [[CrossRef](#)]
29. Pan, J.; He, Y.; Wu, L.; Jiang, C.; Wu, B.; Mondal, A.N.; Cheng, C.; Xu, T. Anion exchange membranes from hot-pressed electrospun QPPO-SiO₂ hybrid nanofibers for acid recovery. *J. Membr. Sci.* **2015**, *480*, 115–121. [[CrossRef](#)]
30. Pan, J.; Ge, L.; Lin, X.; Wu, L.; Wu, B.; Xu, T. Cation exchange membranes from hot-pressed electrospun sulfonated poly(phenylene oxide) nanofibers for alkali recovery. *J. Membr. Sci.* **2014**, *470*, 479–485. [[CrossRef](#)]
31. Güler, E.; van Baak, W.; Saakes, M.; Nijmeijer, K. Monovalent-ion-selective membranes for reverse electro dialysis. *J. Membr. Sci.* **2014**, *455*, 254–270. [[CrossRef](#)]
32. Huang, Z.-M.; Zhang, Y.-Z.; Kotaki, M.; Ramakrishna, S. A review on polymer nanofibers by electrospinning and their applications in nanocomposites. *Compos. Sci. Technol.* **2003**, *63*, 2223–2253. [[CrossRef](#)]
33. Zhang, C.-L.; Yu, S.-H. Nanoparticles meet electrospinning: Recent advances and future prospects. *Chem. Soc. Rev.* **2014**, *43*, 4423–4448. [[CrossRef](#)] [[PubMed](#)]
34. Zhao, W.; Nugay, I.I.; Yalcin, B.; Cakmak, M. Flexible, stretchable, transparent and electrically conductive polymer films via a hybrid electrospinning and solution casting process: In-plane anisotropic conductivity for electro-optical applications. *Displays* **2016**, *45*, 48–57. [[CrossRef](#)]
35. Zhu, Y.; Ahmad, M.; Yang, L.; Misovich, M.; Yaroshchuk, A.; Bruening, M.L. Adsorption of polyelectrolyte multilayers imparts high monovalent/divalent cation selectivity to aliphatic polyamide cation-exchange membranes. *J. Membr. Sci.* **2017**, *537*, 177–185. [[CrossRef](#)]
36. FujiFilm Manufacturing Europe. Curable Compositions and Membranes. BV (NL) Patent C08F 20/36, PCT/GB2012/051569, WO 2013/011273, 24 January 2013.
37. Mizutani, Y.; Yamane, R.; Ihara, H.; Motomura, H. Studies of ion exchange membranes. XVI. The preparation of ion exchange membranes by the “paste method”. *Bull. Chem. Soc. Jpn.* **1963**, *36*, 361–366. [[CrossRef](#)]
38. Doi, S.; Yasukawa, M.; Kakihana, Y.; Higa, M. Alkali attack on anion exchange membranes with PVC backing and binder: Effect on performance and correlation between them. *J. Membr. Sci.* **2019**, *573*, 85–96. [[CrossRef](#)]
39. Hori, Y.; Nakatani, T.; Mizutane, Y. Morphology of ion exchange membranes. *J. Electron. Microsc.* **1986**, *35*, 220–226.
40. Pismenskaya, N.D.; Nikonenko, V.V.; Melnik, N.A.; Shevtsova, K.A.; Belova, E.I.; Pourcelly, G.; Cot, D.; Dammak, L.; Larchet, C. Evolution with time of hydrophobicity and microrelief of a cation-exchange membrane surface and its impact on overlimiting mass transfer. *J. Phys. Chem.* **2012**, *116*, 2145–2161. [[CrossRef](#)] [[PubMed](#)]
41. Nefedova, G.Z.; Klimova, Z.G.; Sapozhnikova, G.S. *Ion-Exchange Membranes, Granulates, Powders: Catalogue*; NIITEKhim: Moscow, Russia, 1977.
42. Rijnaarts, T.; Huerta, E.; van Baak, W.; Nijmeijer, K. Effect of divalent cations on RED performance and cation exchange membrane selection to enhance power densities. *Environ. Sci. Technol.* **2017**, *51*, 13028–13035. [[CrossRef](#)] [[PubMed](#)]
43. Káňavová, N.; Krejčí, A.; Benedeková, M.; Doležel, M.; Machuča, L. Mass transfer examination in electro dialysis using limiting current measurements. *Chem. Pap.* **2015**, *69*, 553–559. [[CrossRef](#)]
44. Safronova, E.Y.; Golubenko, D.V.; Shevlyakova, N.V.; D'yakova, M.G.; Tverskoi, V.A.; Dammak, L.; Grande, D.; Yaroslavtsev, A.B. New cation-exchange membranes based on cross-linked sulfonated polystyrene and polyethylene for power generation systems. *J. Membr. Sci.* **2016**, *515*, 196–203. [[CrossRef](#)]
45. Balster, J.; Krupenko, O.; Pünt, I.; Stamatialis, D.F.; Wessling, M. Preparation and characterisation of monovalent ion selective cation exchange membranes based on sulphonated poly(ether ether ketone). *J. Membr. Sci.* **2005**, *263*, 137–145. [[CrossRef](#)]
46. Sedkaoui, Y.; Szymczyk, A.; Lounici, H.; Arous, O. A new lateral method for characterizing the electrical conductivity of ion-exchange membranes. *J. Membr. Sci.* **2016**, *507*, 34–42. [[CrossRef](#)]
47. Jiang, C.; Wang, Y.; Zhang, Z.; Xu, T. Electrodialysis of concentrated brine from RO plant to produce coarse salt and freshwater. *J. Membr. Sci.* **2014**, *450*, 323–330. [[CrossRef](#)]
48. Karpenko-Jereb, L.V.; Berezina, N.P. Determination of structural, selective, electrokinetic and percolation characteristics of ion-exchange membranes from conductive data. *Desalination* **2009**, *245*, 587–596. [[CrossRef](#)]

49. Tourreuil, V.; Rossignol, N.; Bulvestre, G.; Larchet, C.; Auclair, B. Determination of the selectivity of an ion-exchange membrane - comparison of diffusion flux and transport number. *Eur. Polym. J.* **1998**, *34*, 1415–1421. [[CrossRef](#)]
50. Drioli, E.; Giorno, L.; Fontananova, E. *Comprehensive Membrane Science and Engineering*; Elsevier Science: Amsterdam, The Netherlands, 2017; ISBN 9780444637758.
51. Hannachi, C.; Ali, M.B.S.; Hamrouni, B. Determination of the selectivity coefficient of the CMX cationic membrane at various ionic strengths. *Desalin. Water Treat.* **2009**, *10*, 47–52. [[CrossRef](#)]
52. Długotecki, P.; Anet, B.; Metz, S.J.; Nijmeijer, K.; Wessling, M. Transport limitations in ion exchange membranes at low salt concentrations. *J. Membr. Sci.* **2010**, *346*, 163–171. [[CrossRef](#)]
53. Zhou, J.; Kuang, H.; Zhuang, W.; Chen, Y.; Liu, D.; Ying, H.; Wu, J. Application of electrodialysis to extract 5'-ribonucleotides from hydrolysate: Efficient decolorization and membrane fouling. *RSC Adv.* **2018**, *8*, 29115–29128. [[CrossRef](#)]
54. Jaroszek, H.; Dydo, P. Potassium nitrate synthesis by electrodialysis-metathesis: The effect of membrane type. *J. Membr. Sci.* **2018**, *549*, 28–37. [[CrossRef](#)]
55. Vasil'eva, V.I.; Pismenskaya, N.D.; Akberova, E.M.; Nebavskaya, K.A. Effect of thermochemical treatment on the surface morphology and hydrophobicity of heterogeneous ion-exchange membranes. *Rus. J. Phys. Chem. A* **2014**, *88*, 1293–1299. [[CrossRef](#)]
56. Berezina, N.; Gnusin, N.; Dyomina, O.; Timofeyev, S. Water electrotransport in membrane systems. Experiment and model description. *J. Membr. Sci.* **1994**, *86*, 207–229. [[CrossRef](#)]
57. Gnusin, N.P.; Berezina, N.P.; Kononenko, N.A.; Dyomina, O.A. Transport structural parameters to characterize ion exchange membranes. *J. Membr. Sci.* **2004**, *243*, 301–310. [[CrossRef](#)]
58. Tuan, L.X. Permselectivity and microstructure of anion exchange membranes. *J. Colloid Interface* **2008**, *325*, 215–222.
59. Zabolotsky, V.I.; Nikonenko, V.V. Effect of structural membrane inhomogeneity on transport properties. *J. Membr. Sci.* **1993**, *79*, 181–198. [[CrossRef](#)]
60. Nagarale, R.K.; Gohil, G.S.; Shahi, V.K. Recent developments on ion-exchange membranes and electro-membrane processes. *Adv. Colloid Interface* **2006**, *119*, 97–130. [[CrossRef](#)] [[PubMed](#)]
61. Belashova, E.D.; Melnik, N.A.; Pismenskaya, N.D.; Shevtsova, K.A.; Nebavsky, A.V.; Lebedev, K.A.; Nikonenko, V.V. Overlimiting mass transfer through cation-exchange membranes modified by Nafion film and carbon nanotubes. *Electrochim. Acta* **2012**, *59*, 412–423. [[CrossRef](#)]
62. Kamusewitz, H.; Schossig-Tiedemann, M.; Keller, M.; Paul, D. Characterization of polymeric membranes by means of scanning force microscopy (SFM) in comparison to results of scanning electron microscopy (SEM). *Surf. Sci.* **1997**, *377–379*, 1076–1081. [[CrossRef](#)]
63. Schossig-Tiedemann, M.; Paul, D. Improved preparation of membrane surfaces for field-emission scanning electron microscopy. *J. Membr. Sci.* **2001**, *187*, 85–91. [[CrossRef](#)]
64. Sheldeshov, N.V.; Ganych, V.V.; Zabolotsky, V.I. Transport numbers of salt ions and water dissociation products in cation and anion-exchange membranes. *Sov. Electrochem.* **1991**, *23*, 11–15.
65. Lteif, R.; Dammak, L.; Larchet, C.; Auclair, B. Conductivité électrique membranaire: Étude de l'effet de la concentration, de la nature de l'électrolyte et de la structure membranaire. *Eur. Polym. J.* **1999**, *35*, 1187–1195. [[CrossRef](#)]
66. Karpenko, L.V.; Demina, O.A.; Dvorkina, G.A.; Parshikov, S.B.; Larchet, C.; Auclair, B.; Berezina, N.P. Comparative study of methods used for the determination of electroconductivity of ion-exchange membranes. *Russ. J. Electrochem.* **2001**, *37*, 287–293. [[CrossRef](#)]
67. Nikonenko, V.; Vedernikova, E.; Pismenskaya, N. Device for measurements of diffusion characteristics of membrane. *Rus. Patent* 100275 RF, MPK51 G01N27/40, No 2010121195/28, 10 December 2010.
68. Shutkina, E.A.; Nevakshenova, E.E.; Pismenskaya, N.D.; Mareev, S.A.; Nikonenko, V.V. Diffusion permeability of the anion-exchange membranes in sodium dihydrogen phosphate solution. *Condens. Matter Interphases* **2015**, *17*, 566–578.
69. Larchet, C.; Auclair, B.; Nikonenko, V. Approximate evaluation of water transport number in ion-exchange membranes. *Electrochim. Acta* **2004**, *49*, 1711–1717. [[CrossRef](#)]
70. Gnusin, N.P.; Berezina, N.P.; Shudrenko, A.A.; Ivina, O.P. Electrolyte diffusion across ion-exchange membranes. *Russ. J. Phys. Chem. A* **1994**, *68*, 565.
71. Helfferich, F.G. *Ion Exchange*; ASIN: B0000CLGWI; McGraw-Hill: New York, NY, USA, 1962.

72. Volfkovich, Y.M.; Bagotzky, V.S.; Sosenkin, V.E.; Blinov, I.A. The standard contact porosimetry. *Colloid Surf. A* **2001**, *187–188*, 349–365. [[CrossRef](#)]
73. Kononenko, N.; Nikonenko, V.; Grande, D.; Larchet, C.; Dammak, L.; Fomenko, M.; Volfkovich, Y. Porous structure of ion exchange membranes investigated by various techniques. *Adv. Colloid Interface* **2017**, *246*, 196–216. [[CrossRef](#)] [[PubMed](#)]
74. Kozmai, A.E.; Nikonenko, V.V.; Zyryanova, S.; Pismenskaya, N.D.; Dammak, L. A simple model for the response of an anion-exchange membrane to variation in concentration and pH of bathing solution. *J. Membr. Sci.* **2018**, *567*, 127–138. [[CrossRef](#)]
75. Choi, J.-H.; Moon, S.-H. Structural change of ion-exchange membrane surfaces under high electric field and its effect on membrane properties. *J. Colloid Interface* **2003**, *265*, 93–100. [[CrossRef](#)]
76. Merle, G.; Wessling, M.; Nijmeijer, K. Anion exchange membranes for alkaline fuel cells: A review. *J. Membr. Sci.* **2011**, *377*, 1–35. [[CrossRef](#)]
77. Elattar, A.; Elmidaoui, A.; Pismenskaia, N.; Gavach, C.; Pourcelly, G. Comparison of transport properties of monovalent anions through anion-exchange membranes. *J. Membr. Sci.* **1998**, *143*, 249–261. [[CrossRef](#)]
78. Belova, E.I.; Lopatkova, G.Y.; Pismenskaya, N.D.; Nikonenko, V.V.; Larchet, C.; Pourcelly, G. Effect of anion-exchange membrane surface properties on mechanisms of overlimiting mass transfer. *J. Phys. Chem. B* **2006**, *110*, 13458–13469. [[CrossRef](#)] [[PubMed](#)]
79. Luo, T.; Abdu, S.; Wessling, M. Selectivity of ion exchange membranes: A review. *J. Membr. Sci.* **2018**, *555*, 429–454. [[CrossRef](#)]
80. Hladik, J. *Physics of Electrolytes*; Academic Press: London, UK, 1972; ISBN 10 0123498015.
81. Duke, M.; Zhao, D.; Semiat, R. *Functional Nanostructured Materials and Membranes for Water Treatment*; Wiley-VCH Verlag & Co. KgaA: Weinheim, Germany, 2013; ISBN 978-3-527-32987-8.
82. Vasil'eva, V.I.; Akberova, E.M.; Zabolotsky, V.I.; Goleva, E.A.; Yatsev, A.M. Method of Modification of Sulfonated Cation-Exchange Membrane for High-Intensity Electrodialysis. Rus. Patent 2677202C2 RF, MPK B01D69/00, B01D 61/44, 24 May 2017.
83. Lteif, R.; Dammak, L.; Larchet, C.; Auclair, B. Détermination du nombre de transport d'un contre-ion dans une membrane échangeuse d'ions en utilisant la méthode de la pile de concentration. *Eur. Polym. J.* **2001**, *37*, 627–639. [[CrossRef](#)]
84. Moreno, J.; Grasman, S.; van Engelen, R.; Nijmeijer, K. Upscaling reverse electrodialysis. *Environ. Sci. Technol.* **2018**, *52*, 10856–10863. [[CrossRef](#)] [[PubMed](#)]
85. Akberova, E.M. Structural Effects of Thermochemical Modification of Heterogeneous Ion-Exchange Membranes. Ph.D. Thesis, Voronezh State University, Voronezh, Russia, 2015.



© 2019 by the authors. Licensee MDPI, Basel, Switzerland. This article is an open access article distributed under the terms and conditions of the Creative Commons Attribution (CC BY) license (<http://creativecommons.org/licenses/by/4.0/>).